Multicomponent order parameter superconductivity of Sr_2RuO_4 revealed by topological junctions

M. S. Anwar,[1,*] R. Ishiguro,[2,3] T. Nakamura,[1,4] M. Yakabe,[3] S. Yonezawa,[1] H. Takayanagi,[3] and Y. Maeno[1]

[1]*Department of Physics, Kyoto University, Kyoto 606-8502, Japan*

[2]*Department of Mathematical and Physical Sciences, Faculty of Science, Japan Women's University, Tokyo 112-8681, Japan*

[3]*Department of Applied Physics, Faculty of Science, Tokyo University of Science, Katsushika, Tokyo 162-8601, Japan*

[4]*Institute for Solid State Physics, The University of Tokyo, Kashiwa 277-8581, Japan*

(Received 20 March 2017; revised manuscript received 7 May 2017; published 12 June 2017)

Single crystals of the Sr_2RuO_4-Ru eutectic system are known to exhibit enhanced superconductivity at 3 K in addition to the bulk superconductivity of Sr_2RuO_4 at 1.5 K. The 1.5 K phase is believed to be a spin-triplet, chiral p-wave state with a multicomponent order parameter, giving rise to chiral domain structure. In contrast, the 3 K phase is attributable to enhanced superconductivity of Sr_2RuO_4 in the strained interface region between Ru inclusion of a few to tens of micrometers in size and the surrounding Sr_2RuO_4. We investigate the dynamic behavior of a topological junction, where a superconductor is surrounded by another superconductor. Specifically, we fabricated Nb/Ru/Sr_2RuO_4 topological superconducting junctions, in which the difference in phase winding between the s-wave superconductivity in Ru microislands induced from Nb and the superconductivity of Sr_2RuO_4 mainly governs the junction behavior. Comparative results of the asymmetry, hysteresis, and noise in junctions with different sizes, shapes, and configurations of Ru inclusions are explained by the chiral domain-wall motion in these topological junctions. Furthermore, a striking difference between the 1.5 and 3 K phases is clearly revealed: the large noise in the 1.5 K phase sharply disappears in the 3 K phase. These results confirm the multicomponent order-parameter superconductivity of the bulk Sr_2RuO_4, consistent with the chiral p-wave state, and the proposed nonchiral single-component superconductivity of the 3 K phase.

DOI: 10.1103/PhysRevB.95.224509

I. INTRODUCTION

Spin-triplet superconductivity is rich in physics due to its spin and orbital degrees of freedom compared to ordinary spin-singlet superconductivity. The layered perovskite oxide Sr_2RuO_4 (SRO) is one of the leading candidates of spin-triplet superconductors (TSCs) with a superconducting transition temperature T_c of 1.5 K [1]. Since the discovery of superconductivity in SRO [2], an intensive amount of experimental and theoretical work has been performed to understand the nature of its superconducting order parameter [1,3–5].

Superconductivity of SRO is extremely sensitive even to nonmagnetic impurities [6]. Spin-susceptibility measurements by the nuclear magnetic resonance (NMR) [7] and the polarized neutron scattering [8] below T_c support the spin-triplet scenarios. Recently, invariant spin susceptibility was reconfirmed using Ru and Sr nuclei and O as well [9,10]. The muon spin rotation and magneto-optical Kerr effect evidence the time-reversal symmetry breaking in the superconducting order parameter of SRO [11]. These observations support the chiral p-wave spin-triplet nature of the order parameter that can be represented as $d = \hat{z}(k_x \pm ik_y)$. Recent observations of the long-range proximity effect emerging at the $SrRuO_3$/SRO interface also support the spin-triplet scenario for SRO [4,5]. Because of the orbital phase winding, it is believed that SRO is a typical example of topological superconductors, and gapless states consisting of Majorana fermions are expected to emerge at its boundaries [12–18]. Extensive theoretical work [1] also indicates that the nature of the order parameter of SRO is a chiral p-wave spin triplet with broken time-reversal symmetry, although there are still unresolved issues [19–21].

Twofold degeneracy of chirality leads to the formation of chiral domains with clockwise $(k_x + ik_y)$ and counterclockwise $(k_x - ik_y)$ chiralities in the orbital order parameter. As a result, two chiral domains are naturally separated by a chiral domain wall (chiral DW), like ferromagnetic domain walls in a ferromagnetic material. Recently, the existence of chiral DWs and their dynamic behavior were investigated experimentally and theoretically [11,19,22–28]. Kidwingira *et al.* [22] reported complicated and hysteretic diffraction patterns in Pb/Cu/SRO junctions. They explained their data in the scenario of chiral DW dynamics and suggested a chiral DW size of the order of 1 μm. The size of a chiral domain is controversial, and it may depend on the experimental probe; for example, experiments using the Kerr effect [11], probing the bulk time-reversal symmetry breaking, and using a scanning superconducting quantum interference device [19], probing the local magnetic field due to the edge current, suggested 50 and 0.4 μm, respectively. It is difficult to estimate the upper limit, which can also depend on the quality of the sample. However, recently, Saitoh *et al.* [26] studied the "inversion symmetry" in the magnetic field dependence of the critical current of Nb/SRO junctions while varying the junction size and estimated the domain size to be 5 μm. This value is similar to the value proposed in our previous report [25], in which we investigated Nb/Ru/SRO topological junctions and observed the telegraphic noise attributable to chiral DW motion [25].

A "topological junction" consists of a superconductor that is surrounded by another superconductor in such a way that the difference in phase winding mainly dictates the junction behavior [25,29,30]. Intuitively, transport properties of a topological junction where a spin-singlet superconductor (SSC) is surrounded by a chiral p-wave TSC can also detect

*Present address: London Centre for Nanotechnology, University College London, London, United Kingdom; s.anwar@ucl.ac.uk

the dynamic behavior of the order parameter of the TSC. We have already reported such dynamic behavior in topological junctions that are fabricated using naturally existing Ru metal inclusions inside SRO-Ru eutectic single crystals. Spin-singlet superconductivity is induced in Ru by putting Nb ($T_c = 9$ K) directly onto a Ru inclusion. For utilization of chiral DWs of SRO-based junctions, it is now important to investigate the controllability of chiral DW motion. In this paper, we report our systematic study of current voltage (I-V) characteristics of Nb/Ru/SRO junctions fabricated in different configurations. It is observed that chiral domain dynamics is strictly related to the geometry and size of junctions.

II. EXPERIMENTATION

We fabricated Nb/Ru/SRO micron-sized superconducting topological junctions using SRO-Ru eutectic crystals. Typically, the width of a Ru inclusion is $\sim 2\mu$m, the length is of the order of 1–50 μm, and the depth is about 10 μm [31]. The crystals were grown using a floating-zone method [32]. In a SRO-Ru eutectic crystal, the onset T_c is significantly enhanced up to 3 K. This superconducting phase with enhanced T_c is known as the 3 K phase [31,33]. As suggested by various measurements [1,33], the 3 K phase emerges at the SRO/Ru interface, possibly because of induced local strain on the SRO side, as demonstrated using pure SRO under uniaxial strains [34–36].

Rectangular SRO-Ru substrates of the size $3 \times 3 \times 0.5$ mm^3 were prepared by cutting the crystal along the ac plane and cleaving it along the ab plane. Note that the ab surface of SRO does not show good electrical contact with metals like Nb, Pb, etc., because of its bad adhesion and possible surface reconstruction of the Ru-O octahedra [37]. However, Ru metal inclusions provide good adhesion to develop good electrical contact. On the other hand, epitaxial growth of materials with relatively lower crystal mismatch on SRO can also improve the electrical contact [4,5]. More importantly, a Ru inclusion naturally provides an embedded metal surrounded by a TSC, being quite suitable for developing a topological junction. For these reasons, we used SRO-Ru eutectic crystals.

Next, the ab surface of SRO substrates was polished using diamond slurry with 0.25-μm average particle size. Shortly after, a 300-nm-thick SiO_x layer was deposited on the ab surface using the rf sputtering technique with a backing pressure of $\sim 10^{-7}$ mbar. Such a thick insulating layer guarantees the prevention any pinholes to avoid a short between Nb and Sr_2RuO_4. Then we coated the substrate with the photoresist (TSMR-8800) and exposed the photoresist to maskless lithography based on a UV laser in only selected areas to achieve targeted junction geometries. The exposed resist was removed with TMAH2-83% developer for 120 s. The substrate was rinsed with deionized water for 30 s and dried with N_2 gas. The exposed part of the SiO_x layer was etched away with CHF_3 gas, which opened a window over the desired area that we wanted to use as a junction area. In this process, a fluoride thin film may be generated on the surface of the sample. Therefore, we performed O_2 plasma cleaning of the junction area. The resist was removed using N-methyl-2-pyrrolidone (NMP), and the substrate was cleaned with acetone and isopropanol. In the next step, we prepared the Nb electrodes using a liftoff technique with a bilayer photoresist (LOR-10A and TSMR-8800) and by UV-laser photolithography. Ar-ion etching was performed *in situ* immediately prior to deposition of the Nb layer in order to remove the newly formed RuO_x layer. A 600-nm-thick Nb layer was sputtered with a base pressure of 10^{-9} mbar. Finally, the liftoff was accomplished with NMP.

A natural question is whether we can control the dynamic behavior by changing the junction configurations. To find the answer, we investigated topological junctions with different configurations. The first type is single topological junctions (STJs), in which a Nb electrode was deposited over a full single Ru inclusion, as presented in Figs. 1(a)–1(c). For these junctions, two electrical leads ($\phi = 25$ μm gold wires) were connected with a Nb electrode, and two other leads were connected directly to the side of the eutectic crystal, as shown in Fig. 1(b). We prepared two STJs, one with a 20-μm-long Ru inclusion (big STJ) and another with a 5-μm-long Ru inclusion (small STJ). The second type is a double topological junction (DTJ), in which two separate Nb electrodes were deposited on two parallel Ru inclusions 4 μm apart [see Fig. 1(d)–1(f)]. For DTJs, two electrical leads were connected to each of the Nb electrodes. We prepared two different DTJs: the equal DTJ, where both Ru inclusions are the same size (~ 6 μm long), and unequal DTJ, where one Ru inclusion is 4 μm long and the other is 6 μm long. The third type is edge topological junctions (ETJs), in which one Nb electrode was deposited only on the edge of the Ru inclusion (3×2 μm^2), as shown in Figs. 1(g)–1(i). The lead configuration of this type of junction is similar to that for the STJ [Fig. 1(h)]. Figure 1(j) shows schematically a rectangular Ru inclusion with round tips with total length L and width w. The total length of the straight part is $L_s = 2L_s = 2(L - 2r) = 2(L - w)$, and the total length of the curved part is $L_c = 2\pi r = \pi w$. For all junctions, gold wires for the electrical leads are attached using room-temperature-cured silver paste (Dupont, 4922N). The transport measurements are performed with a ^{3}He cryostat down to 300 mK. The cryostat was magnetically shielded with high-permeability material (Hamamatsu Photonics, mu-metal).

III. RESULTS

A. Temperature-dependent resistance

Figure 2(a) presents the temperature-dependent resistance data for big and small STJs. Different superconducting transitions are observed. The first sharp transition around 9 K corresponds to T_c of Nb that is not much different than the bulk T_c of Nb. It reflects the good quality of the Nb layers. Final transition starts around 2.8 K and is initiated by the 3 K phase that leads to zero resistance close to 1.8 K (1.6 K) for big STJ (small STJ). Normal-state resistance defined at 10 K is of the order of 100–150 mΩ. It indicates the formation of a metallic interface between Ru and Nb. Note that zero resistance is achieved significantly above the $T_{c\text{-bulk}}$ (T_c of the 1.5 K phase) [25]. Figure 2(b) shows the temperature-dependent resistance of the equal DTJ and ETJ, measured with a 30-μA applied current I_a. Multiple transitions are obviously present. For all of these junctions, the first transition occurs at 9 K, corresponding

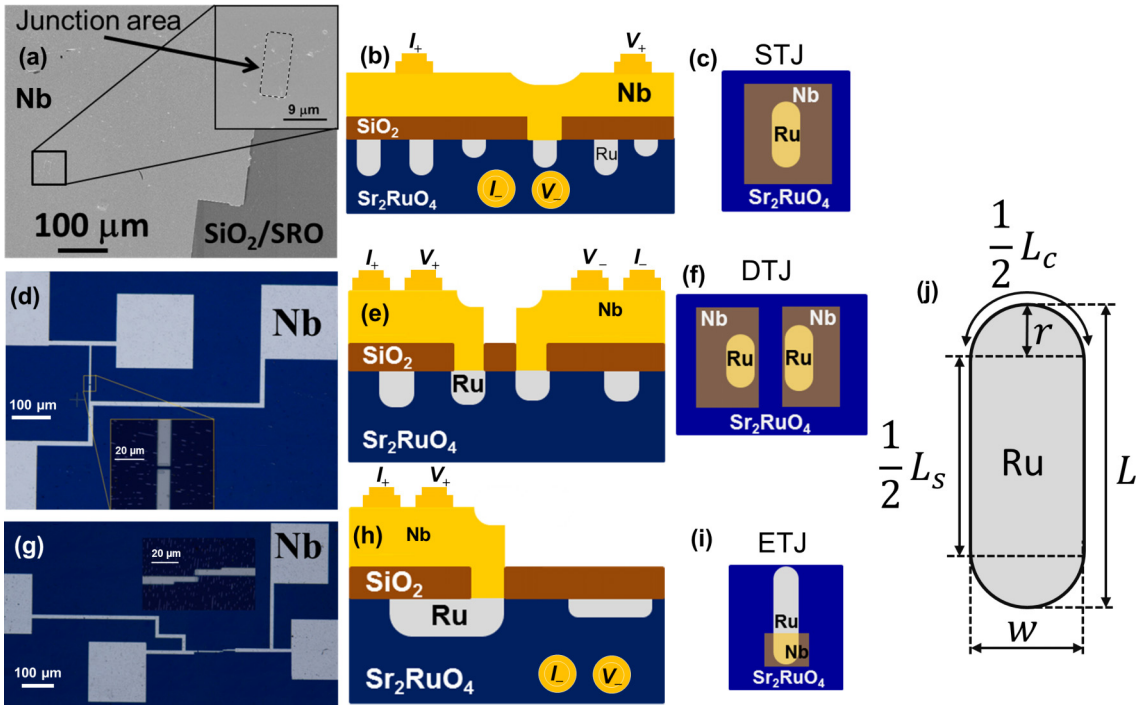

FIG. 1. Three kinds of topological junctions investigated in this study. (a) Scanning electron microscope (SEM) image of a single topological junction (STJ) fabricated using a single Ru inclusion. The inset is a magnified image showing a window over Ru inclusion. (b) Schematic cross-sectional image and (c) top view of the STJ. (d) Optical microscope image of a double topological junction (DTJ) prepared by depositing Nb electrodes onto two parallel Ru inclusions. The inset shows the junction area. (e) Schematic side and (f) top views of the DTJ. (g) Optical microscope image of an edge topological junction (ETJ) made by depositing a Nb electrode only at the edge part of a Ru inclusion. A magnified image around the junction area is shown in the inset. Schematic images of (h) side and (i) top views of the ETJ. (j) Schematic illustration of a single elliptical Ru inclusion of length L and width w. The total lengths of the straight and curved parts are L_s and L_c, respectively.

to superconductivity in the Nb electrodes. However, the second and broad transition appears at 5.8 and 6.5 K for equal DTJ and ETJ, respectively. This second transition arises due to the induction of spin-singlet superconducting correlations in the Ru metal. At lower temperatures, the transition corresponding to the 3 K phase occurs at 1.5 and 2 K for equal DTJ and ETJ, with the zero-resistance transition at 0.9 and 1 K, respectively. These junctions exhibit a zero resistance T_c lower than the ideal T_c of the bulk SRO (1.5 K) due to lower critical current density and/or lower Nb/Ru interface transparency.

Figure 2(c) presents the resistance as a function of temperature for an unequal DTJ. For this junction, we present the resistance data only below 4 K, focusing on the transitions at lower temperatures since the transitions at higher temperatures are similar to those in the other junctions. Interestingly, a sharp transition occurs at 1.75 K for applied current $I_a = 5\ \mu$A (blue triangles). On further cooling, normal-state resistance is recovered at around 1.4 K and jumps to zero resistance at 1.25 K. This anomalous behavior is suppressed with the increase in I_a. Note that the normal-state resistance is robust against an increase in I_a. These facts indicate a strong suppression in the critical current only in the vicinity of the 1.5 K phase transition [29] attributable to topological phase competition between the s-wave and p-wave superconductivities. Such behavior was not observed in other topological junctions studied here. Although such strong suppression was reported in Refs. [29,30], it was not observed in other simpler topological junctions studied here.

B. Current-voltage curves

Figure 3 shows current-voltage (I-V) curves at 0.3 K for the big STJ (black curve) and small STJ (red curve); a schematic of the junction is shown in the inset. Both junctions exhibit asymmetric I-V curves with respect to the direction of the current ($I_{c+} \neq |I_{c-}|$). It is observed that $\Delta I_c = I_{c+} - |I_{c-}| = -40$ and $+19\ \mu$A for the big STJ and small STJ, respectively. The sign and magnitude of the observed asymmetry ΔI_c vary with cooling cycles. Below $T_{c\text{-bulk}}$, the I-V curves in most cases are asymmetric but always become symmetric above $T_{c\text{-bulk}}$ [see Fig. 4(c)]. This asymmetric behavior below $T_{c\text{-bulk}}$ is consistent with the previous observations on Pb/Ru/SRO junctions, where Pb electrodes were deposited on many Ru inclusions [29,30]. If such asymmetric I-V curves arise due to some inhomogeneity or asymmetry at the interfaces of the junction, the asymmetry should not be altered by thermal cycles. On the other hand, some trapped vortices and/or current crowding at the interface can also give rise to asymmetric I-V curves. If that is the case, the asymmetry must present even in the 3 K phase. These effects are in contrast to the present and previous observations [25,29,30]. Thus, the asymmetry is probably attributable to the existence of chiral DWs: our junctions exhibit different chiral DW configurations depending on current sweeps and cooling cycles.

Interestingly, these junctions do not show the same behavior for every cooling cycle. Figure 4(a) represents 16 I-V curves of a big STJ measured consecutively (without disturbing temperature) at 0.3 K during a cooling cycle different from

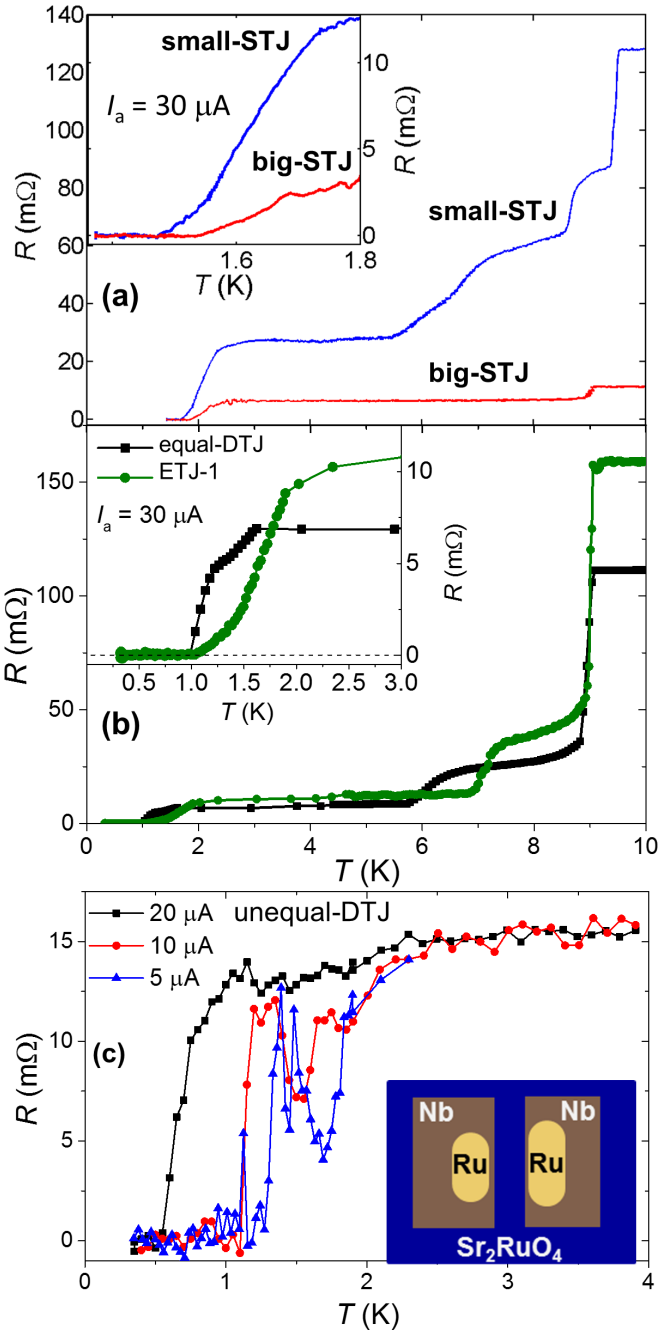

FIG. 2. Junction resistance as a function of temperature. (a) Resistance vs temperature of STJs. Superconducting transitions corresponding to Nb and SRO are observed. (b) Temperature-dependent resistance of the equal DTJ (black points) and ETJ (green points). Data are collected using an Oxford ^{3}He cryostat. The inset shows the resistance at temperatures close to the transition to zero resistance. (c) Resistance vs temperature of the unequal DTJ measured at different applied currents. The inset shows the schematic top view of the junction. These data are obtained using a PPMS ^{3}He probe.

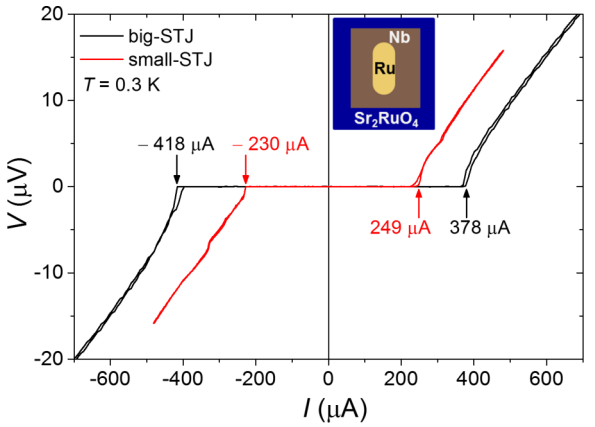

FIG. 3. Asymmetric I-V curves at 0.3 K for big STJ (black) and small STJ (red) in a stable state with small hystereses. Note that the asymmetry is larger for bigger junctions. The inset shows the schematic of the junction.

that presented in Fig. 3. This time, I_c is reduced by more than 50% and is also unstable with variations of more than ~50 μA. These I-V curves also exhibit the unstable and unconventional hysteretic behavior [I_c is smaller than the retrapping current I_r, $I_c < I_r$; see Fig. 4(b)]. Only three I-V curves out of 16 exhibit normal hysteretic behavior ($I_c > I_r$). Note that above I_c there are also additional oscillations [mainly two, indicated by the dotted black lines in Fig. 4(b)]. This oscillation demonstrates that the dynamic behavior is present above the critical current of the junction. Such an unstable and hysteretic behavior is observed only below 1.42 K (1.5 K phase). Figure 4(c) shows two I-V curves measured at 1.5 K during two different cooling cycles, and in both cases the I-V curves are rather stable, with no asymmetry or hysteresis. In order to clarify the temperature evolution of the stability, we investigated the voltage as a function time (telegraphiclike noise) at constant applied current while slowly increasing the temperature from 1.36 to 1.47 K. The applied current is small enough that $V = 0$ even at 1.47 K. One normally anticipates that V stays zero at lower T because I_c increases at lower T. Interestingly enough, Fig. 5 shows that dynamic behavior is strongly suppressed at 1.423 K, $T_{c\text{-bulk}}$ of SRO single crystals used in these experiments. Furthermore, the noise amplitude is higher close to the transition and decreases at lower temperatures with enhanced I_c. The small STJ shows rather stable I-V curves at low temperatures in almost all cooling cycles. However, as represented in Fig. 6(a) at 1.3 K close to the 3 K phase, the I-V curves are persistently and strongly hysteretic with normal behavior ($I_c > I_r$). Interestingly, a sharp and anomalous transition is observed during a current-increasing sweep with negative current. Figure 6(b) presents three consecutive I-V curves at 1.4 K but during another cooling cycle. This time, hysteresis for the positive current is suppressed, but anomalous transitions occur for both forward and backward sweeps of negative current. These results suggest that the stability of topological junctions improves at low temperatures (0.3 K) with the reduction of the junction area, as shown in Fig. 3, but at higher temperatures (close to the 1.5 K phase transition), they are still relatively unstable.

Previously, most of the studies on Pb/Ru/Sr_2RuO_4 junctions used Pb patches deposited over many Ru inclusions. In that case, there are many parallel topological junctions with different cross-sectional areas. In contrast, in the present study and in Ref. [25] the devices consist of well-defined single or double topological junctions. Interestingly, all of these

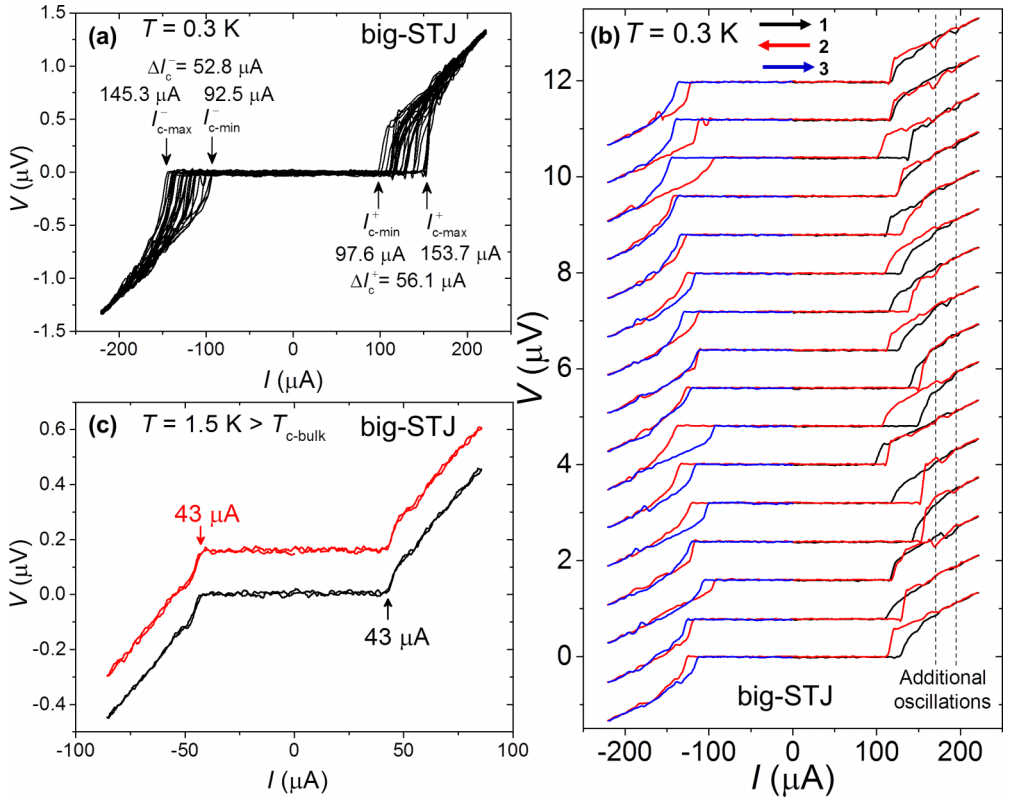

FIG. 4. Unstable and stable behaviors of 1.5 and 3 K phases, respectively, of the big STJ. (a) Sixteen consecutively measured I-V curves at 0.3 K, collected in one cooling cycle where the junction happens to be in an unstable state. Consecutive change in critical current values randomly spread over more than 50 μA. (b) I-V curves shown in (a) with vertical offset illustrating the anomalous hysteretic behavior. Vertical dotted lines indicate the two additional oscillations above the critical current. (c) Two I-V curves at 1.5 K measured during two different cooling cycles. The curves are obviously reproducible, symmetric, and nonhysteretic.

studies result in normal junction behavior only above $T_{\text{c-bulk}}$; below $T_{\text{c-bulk}}$ the junction I_c is unstable, with asymmetric I-V curves. Nevertheless, only weak signatures of I_c suppression are observed in the latter studies with well-defined single or double junctions.

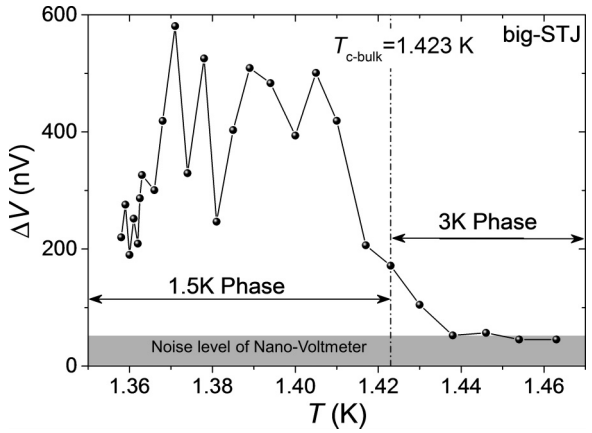

FIG. 5. Amplitude of telegraphiclike noise as a function of temperature of the big STJ. It was suppressed almost down to the noise level of the instruments just above 1.42 K, which is exactly $T_{\text{c-bulk}}$ of the Sr_2RuO_4 crystal.

To further understand and control the dynamic behavior of topological junctions, we investigated the DTJs and ETJs. Figure 7(a) shows the I-V curves of an equal DTJ (a schematic of the junction is given in the inset) measured at 0.3 K for two different cooling cycles. Obviously, strong instability in I_c with a variation of more than $\sim$30 μA is observed in the junctions. I-V characteristics depend on the cooling cycle as well, although the size of one Ru inclusion is 6×2 μm^2 (of the order of the junction area of the small STJ, which is rather stable). In the stable state (black curves), I-V curves are only weakly asymmetric, and no hysteretic behavior is observed. Interestingly, the strong stability is achieved by reducing the size of one of the Ru inclusions down to 4×2 μm^2 (the second Ru inclusion is the same size, 6×2 μm^2). But this junction (unequal DTJ) shows a rather low critical current even at low temperatures [see Fig. 7(b)]. This low critical current is also seen in the resistance behavior: strong suppression of T_c even with 20 μA [Fig. 2(c)]. These results suggest that the instability in the equal DTJ arises due to chiral DW interaction and current distribution around the round parts of both Ru inclusions

Figures 7(c) and 7(d) present I-V curves (five consecutive loops) of two different ETJs with the same junction area (3×2 μm^2). It is clear that for both of these junctions the I-V characteristic curves are persistently stable. There still is a very weak normal hysteretic behavior and asymmetry.

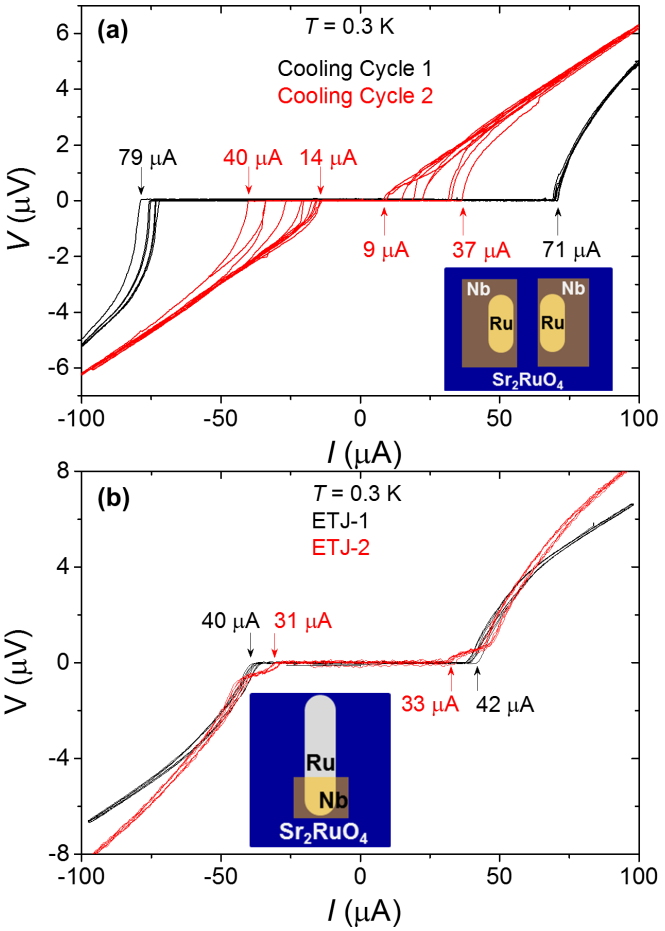

FIG. 6. Relatively stable behavior of the small STJ. (a) Five consecutively measured I-V curves at 1.3 K. All curves exhibit stable behavior with normal hysteresis with positive current, but an anomalous transition appears as current increases for negative current. (b) Three consecutively measured I-V curves at 1.4 K. The hysteretic behavior is suppressed, but the anomalous transition for negative current still occurs.

Nevertheless, these facts suggest that ETJs exhibit higher stability.

IV. DISCUSSION

Before starting our discussion, we briefly summarize our main experimental results related to the stability of our topological junctions fabricated in various configurations. The big STJ in most cases exhibits unstable behavior with ~60% reduction in the critical current compared with that in a stable state. In the unstable state, the I-V curves exhibit unconventional hysteretic behavior ($I_c < I_r$) but only below $T_{c\text{-bulk}}$. Above $T_{c\text{-bulk}}$, the I-V curves are rather stable, symmetric, and nonhysteretic. The stability can be achieved with the reduction of the junction area down to $6 \times 2\ \mu m^2$ for the small STJ. Stability of topological junctions can be controlled also by changing the configuration of the junctions; for example, equal DTJs are unstable relative to unequal DTJs, but the ETJ is completely stable. Note that instability depends on the cooling cycle as well.

Our results reveal that the stability is dependent on junction size; the bigger it is, the more unstable it is, as summarized in Table I. Furthermore, the unstable behavior emerges only below $T_{c\text{-bulk}}$. Such a dynamic behavior is consistently explained by the motion of chiral DWs of the SRO spin-triplet superconductor. Below, we perform calculations using a simple model based on two chiral DWs to simulate our results. We consider two chiral DWs separating two chiral domains with opposite chirality and intersecting a circular Ru inclusion, as illustrated in Figs. 8(a) and 8(b). For simplicity, we fixed one chiral DW, labeled F, at $\theta = 0$, while the other chiral DW, labeled M, at some angle $\theta = \theta_{DW}$ is free to move between stable and metastable states. For such a chiral DW configuration, I_c can be calculated using the following relation [25]:

$$I_c = \max\left[\frac{I_{co}}{2\pi}\int_0^{\theta_{DW}} d\theta \sin\varphi_+(\theta;\theta_{DW},\delta\varphi) + \int_{\theta_{DW}}^{2\pi} d\theta \sin\varphi_-(\theta;\theta_{DW},\delta\varphi)\right], \quad (1)$$

where $\delta\varphi$ is the phase difference at $\theta = 0$ between an s-wave spin-singlet superconductivity (induced in Ru from a Nb electrode) and p-wave spin-triplet superconductivity SRO. For the single-valuedness and symmetry of the order parameter, we consider the phase difference across a chiral DW $\alpha = \pi - \theta_{DW}$ and $\alpha_M = -\alpha_F$ [see Figs. 8(a) and 8(b)], and $\delta\varphi$ is varied so that I_c becomes maximal. Calculated I-V curves using the relation for an overdamped junction and I_c at various θ_{DW} varying from zero to π are given in Fig. 8(c). The sinusoidal variations of I_c as a function of θ_{DW} are shown in the inset. The maximum I_c is found for M at position $\theta_{DW} = \pi$ and $\delta\varphi = \alpha = 0$, as shown in Fig. 8(a). I_c reduces down by 30% for $\theta_{DW} = 0.5\pi$ ($\delta\varphi = 0.25\pi$ and $\alpha = 0.5\pi$); this configuration is shown schematically in Fig. 8(b). The 60% suppression in I_c is achieved at $\theta_{DW} = 0.3\pi$ ($\delta\varphi = 0.35\pi$ and $\alpha = 0.7\pi$); such a reduction corresponds to the small I_c of the big STJ in the unstable state.

Realistically, the Ru inclusions embedded in SRO crystals used in this work are in a rectangular shape with two circular edges and straight parts [see Fig. 1(j)]. The edges must have higher crystal mismatch between SRO and Ru due to larger curvature. Such a mismatch results in a higher pinning potential, providing suitable pinning sites to pin the chiral DWs. In this scenario, the smooth straight parts of Ru inclusions have comparatively lower pinning potential. Therefore, the most stable configuration with maximum I_c is obtained by pinning two chiral DWs at the tips of opposite circular edges of a Ru inclusion. Our simple model calculations also predict that the stability with maximum I_c is obtained when the chiral DW M is pinned at $\theta_{DW} = \pi$. The stability of the junction is disturbed with the increase in the temperature and external magnetic field scans as well [22,25]. But high enough I_c ($\sim 400\mu A$) can itself be a dragging force to move the chiral DWs from a stable state to neighboring metastable states, which results in a reduction and fluctuations in I_c. Nevertheless, it would be difficult to eliminate the chiral DW since the chirality is the degeneracy of the angular momentum direction of Copper pairs and does not couple with electric current strongly. Such dynamic effects could be the origin of the unconventional hysteretic behavior ($I_c > I_r$)

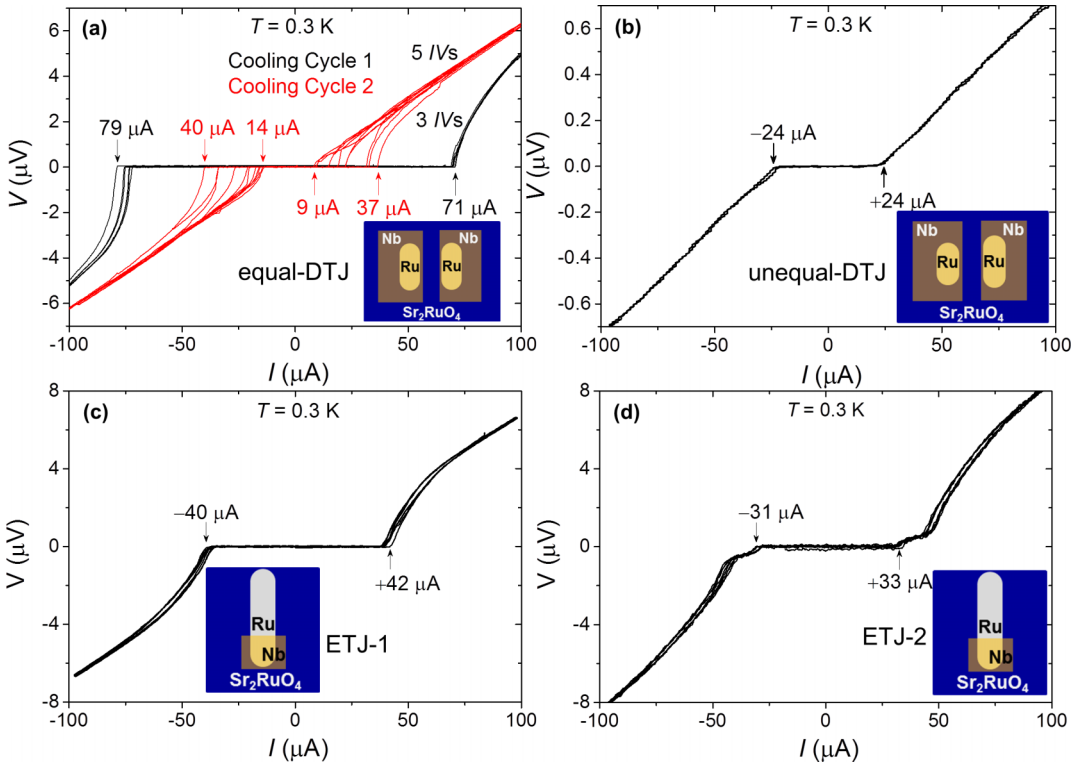

FIG. 7. Unstable and stable behaviors of DTJs and ETJs. (a) Two different sets of I-V curves at 0.3 K measured in two different cooling cycles of an equal DTJ. Black curves with higher I_c are rather stable. In contrast, red curves exhibit lower and strongly unstable I_c values spread over ≈30 μA. (b) Stable and symmetric I-V curves of an unequal DTJ. Five consecutively measured I-V curves of (c) ETJ 1 and (d) ETJ 2. Insets illustrate the top view of corresponding junctions.

and variations in $I > I_c$ by switching a chiral DW to another close-by metastable state. That means chiral DW motion can be initiated in the criticality region (between zero voltage transition and straight Ohmic behavior). This is also supported by the observations of oscillations just above I_c in I-V curves for STJs in the unstable state [see Fig. 4(b)].

The stability in the Nb/Ru/SRO junctions is expected to be achieved by reducing the size of the junction down to the size of the chiral domain. The small STJ with a junction area of 2 × 5 μm^2 is rather stable. This suggests that the size of the chiral domain is of the order of 5 μm [26]. Interestingly, the small STJ shows sharp switching in the I-V curves at 1.3 K only for negative current (Fig. 6). Such an unusual I-V characteristics behavior was already reported by Kambara *et al.* [23,24] in Ru/SRO junctions. Those results were attributed to the current-induced motion of chiral DWs in the 3 K phase.

We summarize the device configuration parameters and results of stability in Table I, which shows that the devices with a higher L_s/L_c ratio are more unstable. This suggests that stability can be achieved by increasing the length of the curved length L_c of the Ru inclusion. On the other hand, Eq. (1) shows that the direction (θ is defined as normal to the Ru/SRO interface) is constant for a flat part and strongly varies for a curved part of the Ru inclusion. In addition, the pinning potential should be lower for the flat part and higher for the curved part due to the larger lattice mismatch along the curvature. These considerations suggest that the stability of Nb/Ru/SRO topological junctions can be controlled by correctly selecting the part of the Ru inclusion on which to place the Nb electrode. These are our results for DTJs and ETJs.

Our systematic investigations suggest that the switching in I_c due to chiral DW motion between neighboring metastable

TABLE I. Properties of junctions at 0.3 K (sorted by the L_s/L_c ratio).

	Ru size (μm^2)	L_s (μm)	L_c (μm)	L_s/L_c	Stable/unstable switching	State	Asymmetry	I-V ordinary hysteresis	I-V unusual hysteresis	Instability
Big STJ	2 × 20	36	6.3	5.7	yes	unstable	yes	yes	yes	yes
						stable	yes	small	no	no
Equal DTJ	2 × 6, 2 × 6	16	12.6	1.3	yes	unstable	yes	yes	yes	yes
						stable	yes	small	no	no
Small STJ	2 × 5	6	6.3	1.0	no	stable	yes	yes	no	small
Unequal DTJ	2 × 6, 2 × 4	12	12.6	1.0	no	stable	no	no	no	no
ETJ 1	2 × 3	2	6.3	0.3	no	stable	small	small	no	no
ETJ 2	2 × 3	2	6.3	0.3	no	stable	small	small	no	no

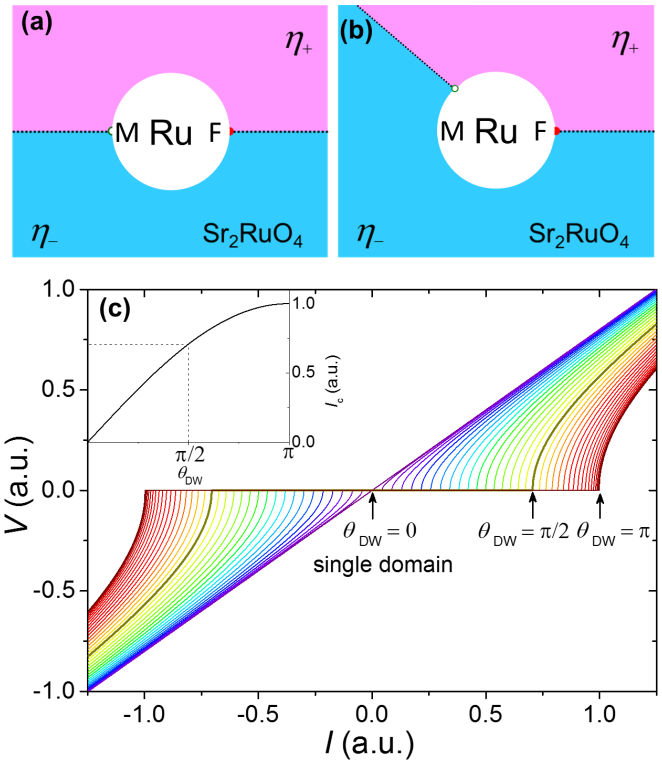

FIG. 8. Critical current based on a model with chiral domain wall (chiral DW) motion for a STJ. (a) Chiral DW configuration for SRO-Ru system: the circular white part is the Ru inclusion surrounded by two chiral domains with different chiralities separated by two chiral DWs; one chiral DW, labeled F, at $\theta = 0$ is assumed to be pinned, and the other chiral DW, labeled M, is at θ_{DW}. Maximum sustainable current can be achieved when pinning M at $\theta_{DW} = \pi$. (b) By pinning M at $\theta_{DW} = \pi/2$, the critical current is reduced by 30%. (c) I-V curves calculated varying θ_{DW} from zero to π. The inset shows the critical current as a function of θ_{DW}.

states can vary I_c by discrete current values rather than continuously. Figure 9 shows a histogram of I_c variations in the big STJ. Note that we include both $+I_c$ and $-I_c$ obtained from the data presented in Figs. 4(a) and 4(b). In an unstable state I_c is mainly distributed between 110 and 140 μA. Furthermore, the I_c variations are not completely continuous, but to claim the discreteness more data may be needed. We leave for future study quantum variations in I_c due to chiral DW motion.

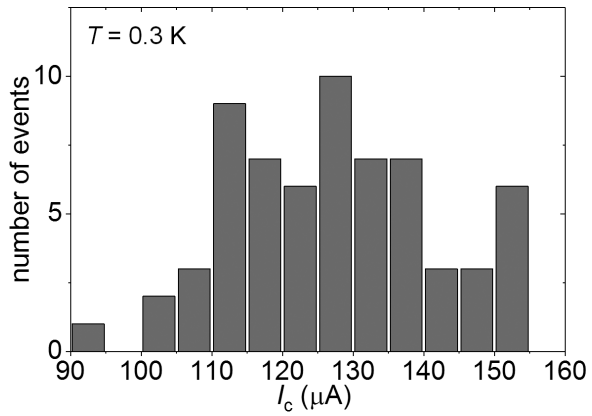

FIG. 9. Histogram of critical current measured from hysteretic I-V curves of the big STJ given in Fig. 4(b).

Recently, Etter *et al.* [38] proposed that transport properties of topological junctions based on the eutectic SRO-Ru system depend strongly on phase winding. They found that in the 3 K phase the phase winding is zero and the junction exhibits ordinary or unfrustrated behavior. However, the phase winding is nonzero (± 1) in the 1.5 K phase, and the junction is frustrated due to the phase mismatch between Ru and SRO. This proposed behavior is similar to our experimental observation. Specifically, this theory suggests stability will be enhanced with an increase in Ru size. In contrast, we observed that larger Ru size shows more unstable behavior.

Before closing our discussion, we would like to comment on the effect of possible vortex trapping. Some vortices can be trapped in the junction even under a very small residual field during cooling down below T_c. The dynamics of such trapped vortices can cause anisotropic I-V curves due to the vortex flow from the Ru/SRO interface to the bulk SRO or vice versa [39]. However, it is difficult to explain the anomalous hysteresis [40] [see Fig. 4(b)]. Furthermore, the vortex flow, if playing a crucial role, should be observable below the onset temperature of the 3 K phase or at least below the temperature where zero resistance emerges (1.8 K in the case of STJs). In contrast, the observed asymmetric I-V curves with anomalous hysteresis and telegraphiclike noise are observed only when the bulk superconductivity in SRO (see Figs. 4 and 5) sets in. In addition, we again emphasize that we cooled down the junctions rather slowly in a zero-field environment prepared by magnetic shielding in order to suppress any significant effect of trapped vortices.

V. CONCLUSION

We investigated Nb/Ru/SRO topological junctions fabricated in various configurations, sizes, and shapes of the Ru inclusions. Such superconducting junctions exhibit contrasting instabilities in the critical currents between the s-wave proximitized Ru and SRO. Junctions with relatively large Ru inclusions are rather unstable and exhibit large noise, asymmetry in the current reversal, and hysteresis in current-sweep loops and on cooling cycles. In contrast, junctions with a size smaller than about 5 μm exhibit ordinary stable I-V characteristics. A striking disappearance of the noisy character is observed when the junction is slowly heated across the bulk $T_{c\text{-bulk}}$ into the 3 K interfacial superconductivity region.

All these results are coherently explained if the bulk superconducting phase (the 1.5 K phase) of SRO has a multicomponent order parameter resulting in a superconducting domain structure. This is consistent with the chiral p-wave superconductivity of the bulk SRO and the nonchiral superconductivity of the 3 K phase. We systematically investigated various junctions, but still more statistics are needed to reach a firm conclusion. Our work will stimulate research work to explore the physics of topological superconducting junctions and the functionality of their dynamic behavior.

ACKNOWLEDGMENTS

We thank S. Kashiwaya, and R. Takashima for fruitful discussions. This work is supported by the Topological Quantum Phenomena (Grants No. JP22103002 and No. JP25103721) and Topological Materials Science (JSPS KAKENHI Grants No. JP15H05851, No. JP15H05852, and No. JP15K21717) on Innovative Areas from the Japan Society for the Promotion of Science (JSPS). M.S.A. is supported as an International Research Fellow of the JSPS.

[1] Y. Maeno, S. Kittaka, T. Nomura, S. Yonezawa, and K. Ishida, J. Phys. Soc. Jpn. **81**, 011009 (2012).
[2] Y. Maeno, H. Hashimoto, K. Yoshida, S. Nishizaki, T. Fujita, J. G. Bednorz, and F. Lichtenberg, Nature (London) **372**, 532 (1994).
[3] A. P. Mackenzie and Y. Maeno, Rev. Mod. Phys. **75**, 657 (2003).
[4] M. S. Anwar, Y. J. Shin, S. R. Lee, S. J. Kang, Y. Sugimoto, S. Yonezawa, T. W. Noh, and Y. Maeno, Appl. Phys. Express **8**, 019202 (2015).
[5] M. S. Anwar, S. R. Lee, R. Ishiguro, Y. Sugimoto, Y. Tano, S. J. Kang, Y. J. Shin, S. Yonezawa, D. Manske, H. Takayanagi, T. W. Noh, and Y. Maeno, Nat. Commun. **7**, 13220 (2016).
[6] N. Kikugawa, A. P. Mackenzie, and Y. Maeno, J. Phys. Soc. Jpn. **72**, 237 (2003).
[7] K. Ishida, H. Mukuda, Y. Kitaoka, K. Asayama, Z. Q. Mao, Y. Mori, and Y. Maeno, Nature (London) **396**, 658 (1998).
[8] J. A. Duffy, S. M. Hayden, Y. Maeno, Z. Mao, J. Kulda, and G. J. McIntyre, Phys. Rev. Lett. **85**, 5412 (2000).
[9] K. Ishida, M. Manago, T. Yamanaka, H. Fukazawa, Z. Q. Mao, Y. Maeno, and K. Miyake, Phys. Rev. B **92**, 100502(R) (2015).
[10] M. Manago, K. Ishida, Z. Mao, and Y. Maeno, Phys. Rev. B **94**, 180507(R) (2016).
[11] J. Xia, Y. Maeno, P. T. Beyersdorf, M. M. Fejer, and A. Kapitulnik, Phys. Rev. Lett. **97**, 167002 (2006).
[12] M. Matsumoto and M. Sigrist, J. Phys. Soc. Jpn. **68**, 994 (1999).
[13] N. Read and D. Green, Phys. Rev. B **61**, 10267 (2000).
[14] M. Stone and R. Roy, Phys. Rev. B **69**, 184511 (2004).
[15] S. Kashiwaya, H. Kashiwaya, H. Kambara, T. Furuta, H. Yaguchi, Y. Tanaka, and Y. Maeno, Phys. Rev. Lett. **107**, 077003 (2011).
[16] X.-L. Qi and S.-C. Zhang, Rev. Mod. Phys. **83**, 1057 (2011).
[17] J. Alicea, Rep. Prog. Phys. **75**, 076501 (2012).
[18] Y. Tanaka, M. Sato, and N. Nagaosa, J. Phys. Soc. Jpn. **81**, 011013 (2012).
[19] C. W. Hicks, J. R. Kirtley, T. M. Lippman, N. C. Koshnick, M. E. Huber, Y. Maeno, W. M. Yuhasz, M. B. Maple, and K. A. Moler, Phys. Rev. B **81**, 214501 (2010).
[20] S. Yonezawa, T. Kajikawa, and Y. Maeno, Phys. Rev. Lett. **110**, 077003 (2013).
[21] E. Hassinger, P. Bourgeois-Hope, H. Taniguchi, S. René de Cotret, G. Grissonnanche, M. S. Anwar, Y. Maeno, N. Doiron-Leyraud, and Louis Taillefer, Phys. Rev. X **7**, 011032 (2017).
[22] F. Kidwingira, J. D. Strand, D. J. V. Harlingen, and Y. Maeno, Science **314**, 1267 (2006).
[23] H. Kambara, S. Kashiwaya, H. Yaguchi, Y. Asano, Y. Tanaka, and Y. Maeno, Phys. Rev. Lett. **101**, 267003 (2008).
[24] H. Kambara, T. Matsumoto, H. Kashiwaya, S. Kashiwaya, H. Yaguchi, Y. Asano, Y. Tanaka, and Y. Maeno, J. Phys. Soc. Jpn. **79**, 074708 (2010).
[25] M. S. Anwar, T. Nakamura, S. Yonezawa, M. Yakabe, R. Ishiguro, H. Takayanagiand, and Y. Maeno, Sci. Rep. **3**, 2480 (2013).
[26] K. Saitoh, S. Kashiwaya, H. Kashiwaya, Y. Mawatari, Y. Asano, Y. Tanaka, and Y. Maeno, Phys. Rev. B **92**, 100504(R) (2015).
[27] A. Bouhon and M. Sigrist, New J. Phys. **12**, 043031 (2010).
[28] Y. Nago, R. Ishiguro, T. Sakurai, M. Yakabe, T. Nakamura, S. Yonezawa, S. Kashiwaya, H. Takayanagi, and Y. Maeno, Phys. Rev. B **94**, 054501 (2016).
[29] T. Nakamura, R. Nakagawa, T. Yamagishi, T. Terashima, S. Yonezawa, M. Sigrist, and Y. Maeno, Phys. Rev. B **84**, 060512 (2011).
[30] T. Nakamura, T. Sumi, S. Yonezawa, T. Terashima, M. Sigrist, H. Kaneysasu, and Y. Maeno, J. Phys. Soc. Jpn. **81**, 064708 (2012).
[31] Y. Maeno, T. Ando, Y. Mori, E. Ohmichi, S. Ikeda, S. NishiZaki, and S. Nakatsuji, Phys. Rev. Lett. **81**, 3765 (1998).
[32] Z. Q. Mao, Y. Maeno, and H. Fukazawa, Mater. Res. Bull. **35**, 1813 (2000).
[33] H. Yaguchi, M. Wada, T. Akima, Y. Maeno, and T. Ishiguro, Phys. Rev. B **67**, 214519 (2003).
[34] C. W. Hicks, D. O. Brodsky, E. A. Yelland, A. S. Gibbs, J. A. N. Bruin, M. E. Barber, S. D. Edkin, K. Nishimura, S. Yonezawa, Y. Maeno, and A. P. Mackenzie, Science **344**, 283 (2014).
[35] H. Taniguchi, K. Nishimura, S. K. Goh, S. Yonezawa, and Y. Maeno, J. Phys. Soc. Jpn. **84**, 014707 (2015).
[36] A. Steppke, L. Zhao, M. E. Barber, T. Scaffidi, F. Jerzembeck, H. Rosner, A. S. Gibbs, Y. Maeno, S. H. Simon, A. P. Mackenzie, and C. W. Hicks, Science **355**, eaaf9398 (2017).
[37] R. Matzdorf, Z. Fang, Ismail, J. Zhang, T. Kimura, Y. Tokura, K. Terakura, and E. W. Plummer, Science **289**, 746 (2000).
[38] S. B. Etter, H. Kaneyasu, M. Ossadnik, and M. Sigrist, Phys. Rev. B **90**, 024515 (2014).
[39] H. K. Lee, Phys. C (Amsterdam, Neth.) **385**, 421 (2002).
[40] W. Yu, K. H. Lee, and D. Stroud, Phys. Rev. B **47**, 5906 (1993).